Structural Correlates for Enhanced Stability in the E2 DNA-Binding Domain from Bovine Papillomavirus[†,‡]

Sudha Veeraraghavan,[§] Cecilia C. Mello,[§] Elliot J. Androphy,[||] and James D. Baleja*[,§]

Department of Biochemistry, Tufts University School of Medicine, 136 Harrison Avenue, Boston, Massachusetts 02111, and Department of Dermatology, Box 166, New England Medical Center, 750 Washington Street, Boston, Massachusetts 02111

Received July 15, 1999; Revised Manuscript Received October 12, 1999

ABSTRACT: Papillomaviral E2 proteins participate in viral DNA replication and transcriptional regulation. We have solved the solution structure of the DNA-binding domain of the E2 protein from bovine papillomavirus (BPV-1). The structure calculation used 2222 distance and 158 dihedral angle restraints for the homodimer (202 residues in total), which were derived from homonuclear and heteronuclear multidimensional nuclear magnetic resonance (NMR) spectroscopic data. The root-mean-square deviation for structured regions of the monomer when superimposed to the average is 0.73 ± 0.10 Å for backbone atoms and 1.42 ± 0.16 Å for heavy atoms. The 101 residue construct used in this study (residues 310−410) is about 4.5 kcal/mol more stable than a minimal domain comprising the C-terminal 85 amino acid residues (residues 326−410). The structure of the core domain contained within BPV-1 E2 is similar to the corresponding regions of other papillomaviral E2 proteins. Here, however, the extra N-terminal 16 residues form a flap that covers a cavity at the dimer interface and play a role in DNA binding. Interactions between residues in the N-terminal extension and the core domain correlate with the greater stability of the longer form of the protein relative to the minimal domain.

Papillomaviruses infect epithelial cells, and certain strains are associated with tumor formation. The 410 amino acid E2 protein of bovine papillomavirus type 1 (BPV-1)[1] regulates viral replication and transcription. The N-terminal half of the molecule contains the transactivating properties of the protein whereas the DNA binding and dimerization functions reside in the last ∼100 residues. The two domains are linked by a presumed flexible tether. Most of the hinge region may be deleted with no effect on the ability of E2 to transactivate (*1*). The shortest construct capable of binding DNA is about 85 residues, which represents the minimal or core DNA-binding domain/dimerization domain (DBD).

X-ray crystallographic structures of the minimal DBD (residues 326−410) in the DNA-free and DNA-bound forms reveal an architecture comprising an eight-stranded β-barrel flanked on two sides by two α-helices. A pair of the α-helices interacts with successive major grooves of DNA, preferring the sequence $ACCGN_4CGGT$, where N is any nucleotide (*2, 3*). The minimal DNA-binding domains of the HPV-31 and HPV-16 E2 proteins bind to the same DNA sequence. The DNA-free structures of these two proteins show a similar structural architecture to the corresponding residues in the BPV-1 E2 crystal structures (*4, 5*). Examination of DNA binding for the minimal domains show that HPV-16 E2 is sensitive to the identity of the middle four base pairs, whereas BPV-1 E2 is indifferent (*6, 7*). Although the structure of HPV-16 E2 in complex with DNA is unknown, in the BPV-1 E2/DNA complex, the DNA is observed to bend smoothly around the protein. Changes in the position of the DNA recognition helices and charge distribution of the DNA-binding surfaces have been correlated with the differences in DNA binding between BPV-1 and HPV-16.

The core DBD of the Epstein Barr Virus transactivating protein EBNA1 comprises residues 504−604 and is structurally homologous to the minimal domain of E2 (*8, 9*). A 45 residue N-terminal extension (residues 459−503) is partially structured and contains an α-helix that projects into the major groove of the DNA. Sequence-specific DNA binding by EBNA1 involves residues both in the core domain and in the N-terminal extension (*10*).

Although most biophysical and biochemical studies of papillomaviral E2 have focused on the minimal DBD, functional analyses on longer forms reveal that residues N-terminal to the minimal DBD of BPV-1 E2 contribute to the DNA binding activity and enhance stability (*11*). The Asp316 to Tyr mutant in the N-terminal region is known to be DNA-binding defective, and the DNA-binding behavior of the Cys340 to Arg mutant in the core DNA-binding domain is dependent on the presence of the N-terminal

[†]Supported by NIH grants AI34918 and RR06282.

[‡] Atomic coordinates have been deposited with the Protein Data Bank, Brookhaven National Laboratories, filename 1dbd.

* To whom correspondence should be addressed. Phone: (617) 636-6867. Fax: (617) 636-2409. E-mail: jbaleja@opal.tufts.edu.

[§] Tufts University School of Medicine. Current address: Department of Molecular Biology, The Scripps Research Institute, 10555 N. Torrey Pines Rd., La Jolla, CA 92037.

[||] New England Medical Center.

[1] Abbreviations: BPV-1, bovine papillomavirus type 1; HPV, human papillomavirus; DBD, DNA-binding domain; EBNA1, Epstein Barr Virus transactivating protein; NMR, nuclear magnetic resonance; TOCSY, total correlation spectroscopy; DQF-COSY, double-quantum-filtered correlation spectroscopy; NOE, nuclear Overhauser effect; NOESY, nuclear Overhauser effect spectroscopy; HSQC, heteronuclear single quantum coherence; HMQC, heteronuclear multiple quantum coherence; RMS deviation, root-mean-square deviation.

10.1021/bi991633x CCC: $18.00
Published on Web 11/12/1999

extension. Constructs of E2 DNA-binding domains containing an additional 16 or 40 amino acid residues N-terminal to the core domain of 85 amino acid residues are more stable to denaturation by urea (*11*).

The shorter 101 amino acid residue construct includes Asp316 and Cys340 and is as stable as the 125 amino acid residue construct; of the three forms of E2, it was the best target for structure determination using NMR methods. The solution structure reported here suggests a role for the additional N-terminal residues in complementing the DNA-binding functions of the core domain and reveals why the longer forms are more stable than the minimal DNA-binding domain. The insights gained from the structure-stabilizing interactions have implications in previous biophysical measurements made with the minimal DNA-binding domains. In addition, the NMR data complements the previous crystallographic work on the BPV-1 E2 core domain by providing information on residue dynamics in solution.

EXPERIMENTAL PROCEDURES

Sample Preparation. The construct encoded residues 310−410 of BPV-1 E2 DBD (Swiss-Prot P03122) with two additional residues at the N-terminus (Met-Ala) introduced from the cloning procedure. Proteins were expressed and purified as described previously (*12, 13*). N-Terminal sequencing of purified protein showed removal of the methionine (75%) or both N-terminal residues (25%). Purified protein was lyophilized and stored at −20 °C until used. Heterodimeric protein made of ^{13}C-labeled and unlabeled monomers (a ^{12}C,^{13}C -labeled sample) was made by preparing an equimolar mixture of the homodimers at 50 μM concentration in 9 M urea, rapid dilution, and subsequent concentration to 1.7 mM protein (*1, 5*).

Chemicals utilized in sample preparation were reagent grade. Perdeuterated dithiothreitol (DTT-d_{10}) and D_2O (99% or 99.96%) were obtained from Cambridge Isotope Laboratories (Andover, MA). Sample conditions were 1.7−4.5 mM protein, 20 mM sodium phosphate, 0.1 M NaCl, 50 μM EDTA, 5 mM DTT-d_{10}, and 0.01% NaN_3 at pH 5.75 ± 0.1 and 35 °C. Protein samples were layered with argon prior to capping and sealing the NMR tube and were stable for at least 1 week at 35 °C and 4 weeks at 4 °C.

The protein−DNA complex was prepared by gradual addition of ^{15}N-labeled BPV-1 E2 DBD to 18-mer palindromic double-stranded DNA of the sequence 5′-CCGACCGACGTCGGTCGG-3′. The final protein concentration was 0.35 mM and the DNA concentration was 0.4 mM. A small amount of precipitate was observed at addition that disappeared upon mixing the sample gently. All other conditions were as described above.

Stability of BPV-1 E2 DBD. Urea-induced unfolding curves for the 85-, 101-, and 125 residue forms of E2 (*11*) were fitted using Origin software (Microcal, Inc., Amherst, MA) to an equation corresponding to the unfolding of a dimeric protein to two monomers (*14*).

NMR Spectroscopy and Resonance Assignments. NMR resonance assignments for the ∼23 kDa BPV-1 E2 DBD were made using homonuclear and heteronuclear multidimensional spectra collected on Bruker AMX-500 and Avance-600 NMR spectrometers (*13*). Spectral widths were approximately 7500, 2000, and 10 000 Hz, in the ^{1}H, ^{15}N, and ^{13}C dimensions, respectively. The homonuclear 2D data sets were acquired with 2K × 512 points; the ^{1}H-^{15}N and ^{1}H-^{13}C HSQC experiments were acquired with 128 increments. A 3D ^{13}C-filtered, ^{13}C-edited HMQC-NOESY data set was acquired on a ^{12}C,^{13}C-labeled sample using the pulse program described by Vuister et al. (*15*). These data showed intersubunit NOE cross-peaks. The ^{1}H dimension was referenced with respect to water at 4.66 ppm at 35 °C and the ^{15}N and ^{13}C dimensions were referenced using the ratio of gyromagnetic ratios of nitrogen or carbon to proton (*16*). The centers of the nitrogen and carbon dimensions were 116.5 and 47.5 ppm, respectively. Forward linear prediction was used to improve spectral resolution in the ^{15}N and ^{13}C dimensions of the 3D data.

The pK_a values for the four histidine residues were determined by collecting one-dimensional spectra in D_2O solution between pH* 5 and 8 (direct meter value) and following the Hϵ1 resonance positions as a function of pH. The data were fit with a nonlinear regression analysis using Origin software as described elsewhere (*17*).

Structure Calculation. NOE cross-peak intensities determined from homonuclear 2D NOESY and heteronuclear 3D (^{15}N-separated and ^{13}C-separated) NOESY spectra were used in structure calculation. NOE cross-peak intensities were designated as strong (2.5 Å), medium (3.5 Å), or weak (4.5 Å). The corresponding lower bounds were 1.7, 2.7, and 3.7 Å, whereas the upper bounds were 3.0, 4.0, and 5.0 Å, respectively. Upper bounds were increased by 1.1 Å for the pseudoatoms corresponding to methylene and methyl protons, 2.1 Å for pseudoatoms of the 6 methyl protons of Leu and Val, 2.4 Å for the pseudoatoms corresponding to the δ or ϵ protons of Tyr and Phe rings, and 0.5 Å to correct for spin diffusion and overlapping resonances (*18*).

The ϕ dihedral angles for 79 of 101 residues were obtained by measuring coupling constants (±1 Hz) from 1D slices of a ^{1}H-^{15}N HSQC spectrum that was resolution enhanced by applying a 20° shifted squared sine bell over 2K real points in t_2 (*19, 20*). Line widths in the resolution-enhanced spectra were about 5 Hz. Stereospecific assignments for three of four Val methyl groups were determined from NMR data collected using a 10% ^{13}C-labeled protein sample (*21*). Cross-peaks involving Leu methyl groups were weak and precluded stereospecific assignment. Stereospecific assignments of β-protons and $\chi - 1$ torsion angles were determined from $^3J_{H\alpha-H\beta}$ coupling constants and the intensities of NOE cross-peaks between α and amide protons to the β-protons (*22*).

The Biosym suite of software containing Insight II, NMRchitect, and DGII was used in the structure calculation of a monomer of the BPV-1 E2 DBD. Ten initial structures generated by distance geometry and simulated annealing methods were found to have RMS deviation values of less than 2 Å over the backbone of residues 326−360 and 370−400. Distance violations greater than 0.3 Å were compiled from the 10 structures. The upper or lower bounds of the restraints were expanded to reflect the uncertainty in the distance restraints corresponding to overlapping or very weak peaks and a second round of 10 structures was generated. The monomer structure with the lowest energy was energy minimized and duplicated to approximate the dimer structure of E2 for input into X-PLOR (ver. 3.85).

The X-PLOR calculations on the dimer used 2222 unambiguous interproton distance restraints, 158 ϕ dihedral

Table 1: Stability of the BPV-1 E2 DBD[a]

	residues 326−410	residues 310−410	residues 286−410
$\Delta G_u(H_2O)$ (kcal/mol)[b]	8.36 ± 0.29	12.97 ± 0.59	13.38 ± 1.24
$\Delta\Delta G_u(H_2O)$ (kcal/mol)[b]	(0.0)	4.6	4.9
m (L kcal/mol^2)[c]	1.14 ± 0.12	1.79 ± 0.17	1.83 ± 0.34
C_m (M)[c]	1.27 ± 0.4	3.44 ± 0.05	3.56 ± 0.08
χ^2	0.000 36	0.000 45	0.001 26

[a] Data were extracted from the urea-unfolding curves reported by Pepinsky et al. (*11*) by nonlinear least-squares curve fitting. Fitting the urea denaturation data to a model in which a dimeric native protein unfolds to yield two monomeric subunits gave the lowest χ^2 (goodness of fit) values. The protein concentration was 10 μM and the temperature was 25 °C. Three different constructs of BPV-1 E2 DBD were used to prepare the 85 residue form (residues 326−410), the 101 residue form (residues 310−410), and the 125 residue form (residues 286−410) (*11*). [b] The free energy of unfolding in water [$\Delta G_u(H_2O)$] is the ΔG_u value extrapolated to 0 M urea. $\Delta\Delta G_u(H_2O)$ is the free energy difference between a long form and the shortest form. [c] m and C_m correspond to the slope of the unfolding curve and the concentration of denaturant at the midpoint of the transition region.

torsion angle restraints, and 192 α- and β-carbon chemical shift restraints. NOE, dihedral, carbon chemical shift, and noncrystallographic symmetry restraints were used in all calculations including energy minimization protocols. The lower bounds of the NOE cross-peaks were all set to 1.8 Å. Force constants of 50 kcal/mol/Å^2 and 200 kcal/mol/rad were used for the soft-well NOE and for dihedral angle restraints, respectively. The noncrystallographic symmetry force constant was 300 kcal/mol/Å^2. Structure calculations using X-PLOR used simulated annealing and energy minimization protocols followed by two rounds of refinement for 50 annealed structures. Further refinement gave little or no improvement in the energy values or structures. Forty-two structures were identified with NOE violations of less than 0.15 Å and with dihedral violations of less than 5°. Of these, a set of 20 representative energy minimized structures was selected and further analyzed.

RESULTS

Stability to Urea Denaturation. Urea-induced unfolding for the 85-, 101-, and 125 residue forms of E2 has been monitored using fluorescence spectroscopy by Pepinsky et al. and analyzed qualitatively (*11*). The 101 amino acid residue and 125 residue forms of BPV-1 E2 DBD were found to be more stable than the 85 residue core domain. We quantified the native-state stabilities by refitting the urea denaturation data to a model in which a dimeric native protein unfolds to yield two monomeric subunits to derive accurate measurements for the free energy of unfolding and the 50% denaturation point (*14*). Both of the longer forms are 4.6−4.9 kcal/mol more stable than the 85 residue form and both require approximately 2 M more urea to achieve 50% denaturation (Table 1). This indicates the structure-stabilizing factors reside within the 16 residues immediately flanking the N-terminus of the 85mer core DBD.

NMR Spectroscopy and Assignments. Although the E2 DBD is a homodimer of 101 (or 102) amino acid monomers (~23 kDa), the homonuclear 2D spectra were sufficiently resolved allowing identification of side-chain resonances for about 70% of the residues (*19*). Ala, Val, Gly, Leu, Phe, and Lys resonances (40 residues) were identified from ^{15}N-filtered TOCSY and NOESY, and ^{1}H-^{15}N HSQC spectra were acquired with selectively labeled protein (*12*, *13*). Sequential backbone assignments were made using ^{1}H-^{15}N HSQC and 3D ^{1}H-^{15}N-^{1}H NOESY-HSQC data obtained with uniformly ^{15}N-labeled protein. ^{1}H-^{13}C HSQC and ^{1}H-^{13}C-^{1}H HCCH-TOCSY data were used on uniformly ^{13}C-labeled protein to determine the carbon chemical shifts and to identify or confirm the chemical shifts of carbon-bound side-chain protons. Sequence-specific assignments were made for all backbone and side-chain ^{1}H, ^{15}N, and ^{13}C atoms except the carbonyls and protonated amino groups.

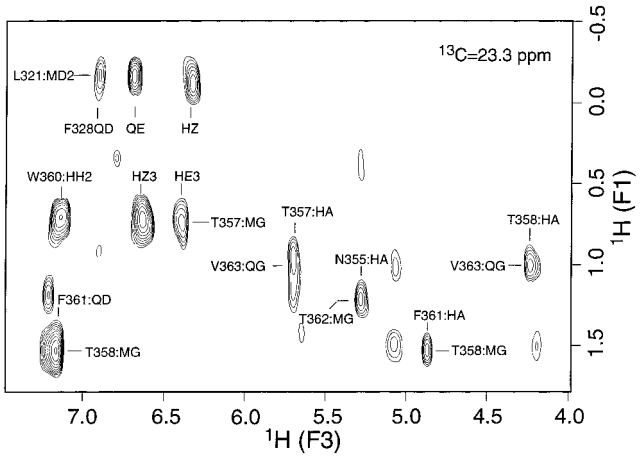

FIGURE 1: Intermonomer NOEs. A slice corresponding to carbon chemical shift of 23.3 ppm is taken from a ^{13}C-filtered, ^{13}C-edited ^{1}H HMQC-NOESY NMR spectrum of BPV-1 E2 DBD (residues 310−410). Cross-peaks that appear strongest in this slice are labeled. Three cross-peaks seen at the upper left correspond to one of the methyl groups of Leu321 in the N-terminal extension of one subunit interacting with the ring protons of Phe328 in the core domain of the other subunit.

Chemical shift index analysis of Hα- and Cα-resonances indicated that the same secondary structural features observed in the minimal domains of E2 proteins were also present in this longer form of the E2 DBD (*23*, *24*). The Hα- and Cα-chemical shifts for the N-terminal extension (residues 310−325) did not indicate any regular secondary structure.

Because the BPV-1 E2 DBD is homodimeric, intramonomer NOE cross-peaks needed to be distinguished from intermonomer cross-peaks. A ^{13}C-selected, ^{13}C-filtered 3D ^{1}H-^{13}C-^{1}H HMQC-NOESY experiment was run on a ^{12}C,^{13}C-labeled protein (*15*). In this experiment, NOE cross-peaks are observed if a proton attached to a ^{12}C isotope in one monomer is within about 5 Å to a proton attached to a ^{13}C isotope in the other monomer. A portion of one slice of the 3D data is shown as Figure 1. In total, the 3D data set reveals the presence of 176 unambiguous intermonomer NOEs for the dimer, most of which correspond to the interactions at the dimer interface observed in the crystal structures of BPV-1 E2 DBD (*2*, *4*). More important for the structure determination of the 101 residue form of E2, intermonomer NOEs to residues in the N-terminal extension were also identified. For example, the methyl groups of Leu321 for one monomer are close to the aromatic ring of Phe328 of the other monomer (Figure 1). One of the methyl groups of Leu321 is substantially shifted upfield (−0.12 ppm), consistent with its position perpendicular to the aromatic ring. Other 2D and 3D NOESY data reveal that His319 in the N-terminal extension makes intersubunit contacts with

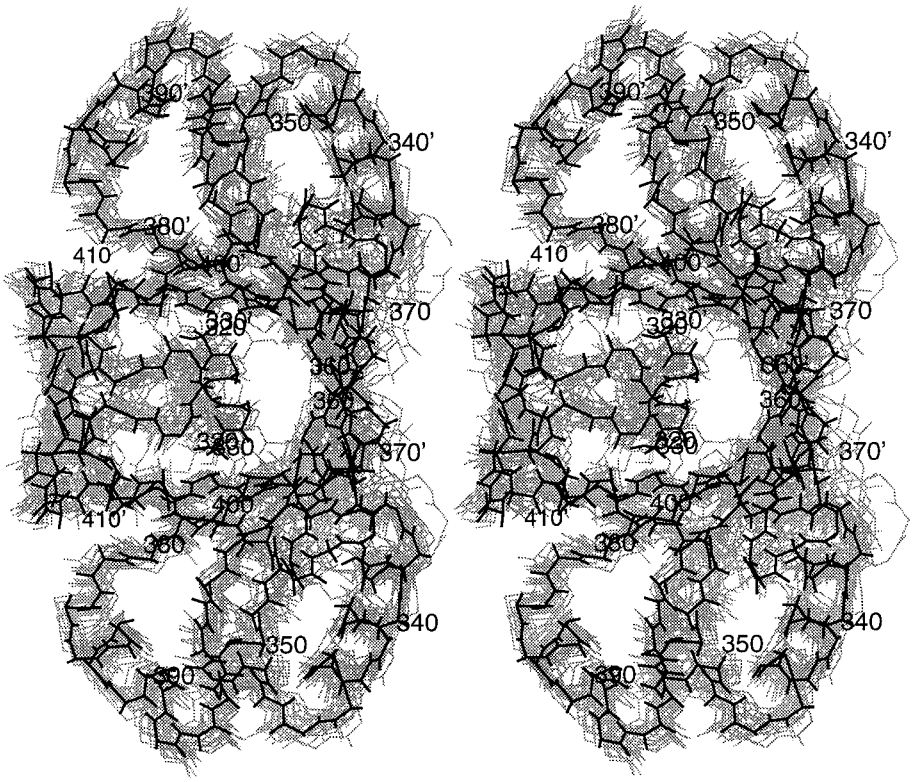

FIGURE 2: Stereoimage of a bundle of 20 BPV-1 E2 DBD (310−410) homodimeric structures (gray, thin lines) superimposed to their average (black, thick lines). Every 10th amino acid is labeled starting from 320. Only residues 317−410 are shown. Residues from the second monomer are labeled with a prime (′). The DNA-recognition helices are located at the right-hand side of the molecule. The RMS deviation to the average (dimer) is 0.95 ± 0.15 Å for backbone atoms of 319−322, 327−361, and 374−397.

Leu330, Ile331, and Ile401 and that Arg322 is near Ile401 and Phe404 of the other subunit.

Solution Structure Determination. A total of 1111 NOE-derived distance restraints per monomer and 79 ϕ restraints described the BPV-1 E2 DBD structures. The distance restraints between two residues, *i* and *j*, include 414 intraresidue contacts ($i - j = 0$), 349 short-range ($i - j = 1$), 54 medium-range ($2 < i - j < 4$), 188 long-range ($i - j \geq 5$), and 88 unambiguous intermonomer restraints (See Supporting Information). Also included were 18 hydrogen-bond restraints corresponding to the slowest hydrogen-exchanging amide protons (amide intensities observed 20 h after solvent exchange).

An ensemble of 20 representative structures and their average is presented in Figure 2. All distance violations were less than 0.15 Å, and dihedral violations were less than 3.5°. These structures, energy minimized using CHARMM-22 force fields (*25*, *26*), have negative total energies with large negative contributions from van der Waals components (Table 2). The electrostatic component also contributes to the negative energies. Positive energy contributions are due to small distance and angle violations distributed throughout each molecule. Noncrystallographic symmetry restraints contribute to about 1 kcal/mol to the total free energies. The low RMS deviations from idealized covalent geometry reflect the high quality of the structures.

The RMS deviation for the backbone atoms of structured residues 327−363 and 374−406 on the average structure is 0.68 ± 0.11 Å for the superimposition onto the monomer and 0.93 ± 0.17 Å for the dimer (Table 2). It is 0.73 ± 0.10 and 0.95 ± 0.15 Å, respectively, when residues 319−321 are also included (Figure 2). The RMS deviation is 0.6−0.7 Å higher when the non-hydrogen atoms of the side chains for the corresponding residues are included. The secondary structural components and the overall conformation of the

Table 2: Structural Statistics for BPV-1 E2 DBD

no. of residues giving NOEs	196
total number of distance restraints	2222
average number of distance restraints per residue	11.4

X-PLOR Energies (kcal/mol) and RMS Deviation from Idealized Covalent Geometry

	ensemble of 20 structures	average structure
E_{total}	−1355 ± 178	−1892
E_{bonds}	164 ± 6	158
E_{angle}	537 ± 23	612
E_{impr}	27.3 ± 3.8	39
E_{noe}	9.9 ± 2.0	8.8
E_{cdih}	4.1 ± 0.7	4.2
E_{vdw}	−535 ± 40	−535
bonds (Å)	0.013 ± 0.000	0.013
angles (deg)	2.27 ± 0.066	2.52
impropers (deg)	2.26 ± 0.24	3.17

RMS Deviation Relative to Average Structure

residues superimposed	backbone atoms (Å)	all heavy atoms (Å)
monomer		
327−361, 374−407	0.68 ± 0.11	1.28 ± 0.12
319−321, 327−361, 374−407	0.73 ± 0.10	1.42 ± 0.16
dimer		
327−361, 374−407	0.93 ± 0.17	1.42 ± 0.16
319−321, 327−361, 374−407	0.95 ± 0.15	1.43 ± 0.15

[a] Numbers correspond to data per dimer, unless otherwise indicated.

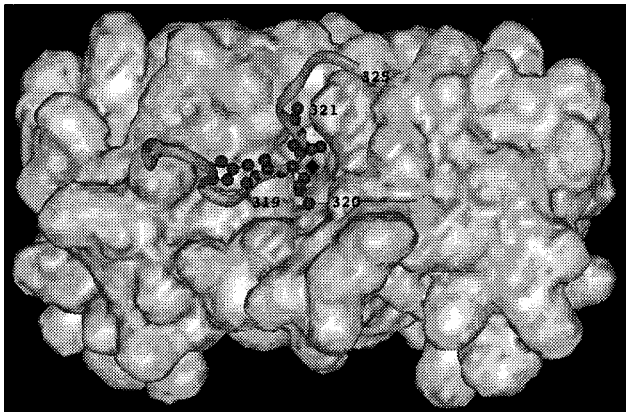

FIGURE 3: Surface of the core DBD (326−410) is shown in gray and the N-terminal residues (310−325) are shown as a ribbon. The side chains of His319, Leu320, and Leu321 are in ball-and-stick to illustrate their positions relative to the central cavity in the E2 homodimer.

85 core residues (326−410) are identical, within experimental error, to the known BPV-1 E2 DBD structures in the DNA-bound and DNA-free states. The homodimeric structure is made up of an eight-stranded β-barrel with two DNA-recognition α-helices on the right-hand side at the top and bottom, and on the left-hand side, another two shorter α-helices. Residues 317−325 in the N-terminal extension take on a distinct backbone conformation and form a flap that covers the primarily hydrophobic dimer interface (Figure 3).

Structured regions in the protein models were identified by consistency in backbone dihedral angles. The backbone angles are best-defined ($S > 0.9$) for residues 319, 328−346, 349−351, 354−361, 374−396, and 399−406 (*27*). Residues with disordered backbone are 310−316, 322, 326, 327, and 364−372. The energy-minimized average of the ensemble was used in further analyses. A total of 97% of structured residues of the average model exists in favored (77.1%) and additionally favored (20.0%) regions of Ramachandran ϕ, ψ space (*28*).

Three histidines of BPV-1 E2, residues 319, 351, and 392, have pK_a values of 6.44 ± 0.03, 5.57 ± 0.02, and 6.43 ± 0.03, respectively. The typical change in chemical shift observed in a histidine titration is 0.7 ppm, and the Hϵ1 resonance of the fourth histidine, residue 349, moves about +0.1 ppm at pH* values approaching 5. Therefore, we estimate its pK_a to be about 4.5. The histidine titration data is consistent with the determined structure. The pK_a for the imidazole group of the amino acid histidine is 6.0 (*29*). Histidines in the vicinity of positively charged amino acids would be expected to have lower pK_a values, whereas histidines near negatively charged amino acids would be expected to have higher pK_a values. All the histidines in BPV-1 E2 are solvent accessible. His319 does not appear to form hydrogen bonds or interact with charged groups and has a pK_a close to that of free histidine. His392 is near Asp388 (~4 Å) and Arg352 (~5 Å), and the charge effects presumably cancel out. His351 appears near Arg352 (~4 Å) and exhibits a slightly higher pK_a. The side chain of His349 is near Arg352 (~5 Å) and Arg354 (6.5 Å). In the crystal structure of BPV-1 E2, which might be expected to have higher resolution, His349 is slightly closer to Arg352 (~2.5 Å) and is partially buried with its δ2 nitrogen forming a hydrogen bond with Hϵ of the arginine (*2*). Ionization of this histidine would be unfavorable and results in the observed shifting of its pK_a by about 1.5 pH units. At pH values less than 5, the protein irreversibly denatures (not shown), suggesting that the neutral form of His349 is required for protein stability.

The conformation of the N-terminal segment is driven primarily by the proximity of residues His319 and Leu321 to residues at the dimer interface (Figure 3). The side chain of Leu321 is oriented toward the central cavity at the dimer interface allowing interactions with Phe328. The His319 side chain is situated to one side of the cavity and interacts with the side chains of residues in β-strands 1 and 4. The anchoring of His319 and Leu321 near the central cavity results in the formation of a substructure (residues 317−325 of each monomer) that interacts with each surface of the dimer interface.

To determine if residues in the 16 amino acid N-terminal extension interact with DNA or were influenced by DNA binding, we compared the ^{1}H-^{15}N HSQC spectrum of the DNA-bound homodimeric E2 DBD (310−410) to that of the DNA-free protein (Figure 4). Since the affinity of BPV E2 for DNA is high (*7*), the complex is in slow exchange. The complex is spectroscopically well-behaved—as many peaks are observed for the DNA-bound form as for the DNA-free form. Since the maximum concentration of complex attainable appears to be only ~0.3 mM and because the complex is rather large (ca. 37 kDa), assignments for the DNA-bound form of E2 could not be obtained using standard assignment methods. What is unambiguous, however, is that resonances for several residues of E2 shift upon DNA. Some assignments for the DNA-bound form were possible by comparing resonances of residues resistant to amide exchange (see Supporting Information). These resonances were well dispersed and showed little change in chemical shifts. Some assignments were also made from a ^{15}N-Gly,^{15}N-Ala-labeled sample. The remaining assignments were made more tentatively by choosing the nearest unassigned peak in the DNA-bound spectrum to the assigned peak in the DNA-free spectrum to indicate the minimum change in chemical shift.

DISCUSSION

Protein engineering has been used to dissect interactions that stabilize or destabilize the structures or modify functions of proteins. However, distinctions between loss of function due to loss of an essential active-site residue versus modification of native-state structure are available for only a handful of proteins (*30*, *31*). Further general principles need to be developed before proteins can be altered to achieve a desired function or to impart structural stability. Of the many types of protein functions, one has emerged to have general importance in cellular signaling—namely, the binding of a protein to its signaling partners such as other proteins, small molecules, or DNA. In this study, we examine how the boundaries of a DNA-binding domain correlate with its presumed function.

The E2 proteins from different strains of papillomaviruses bind palindromic DNA with a required sequence of ACCgN4cGGT (the lower case letters indicate preferred bases and N_4 refers to a spacer of four bases). Binding affinities are known to be dependent on the identity of the

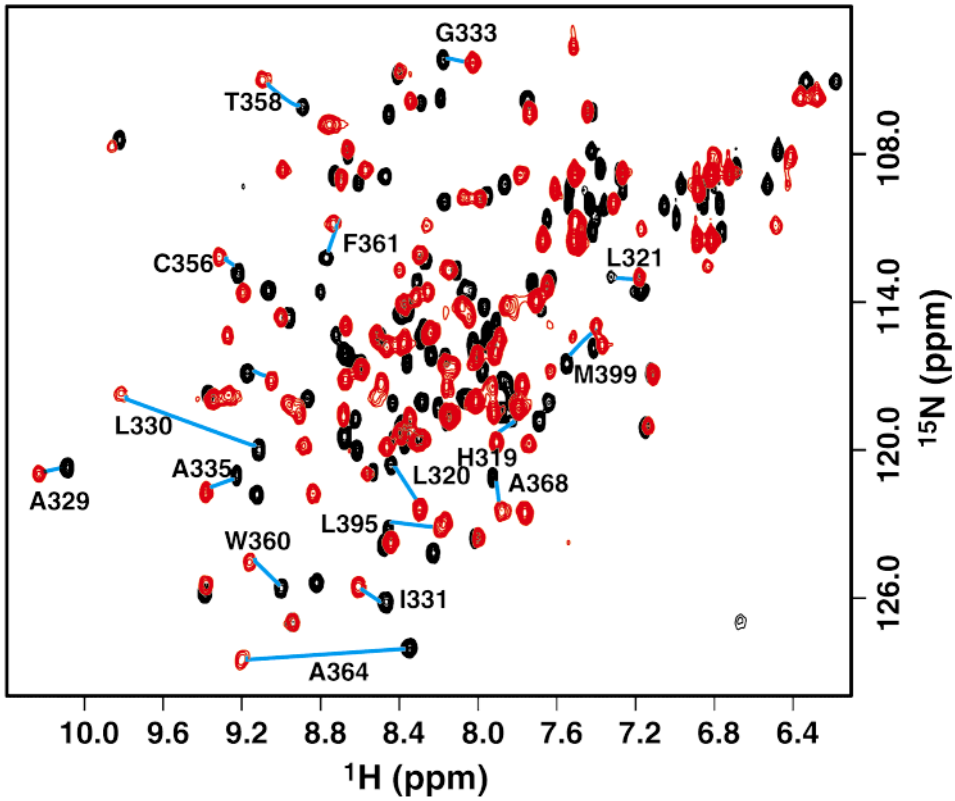

FIGURE 4: ^{1}H-^{15}N HSQC spectra of BPV-1 E2 DBD (310−410). Resonances of the DNA-bound protein (red) show chemical shift differences relative to the DNA-free sample (black). Complete resonance assignments for the DNA-free E2 have been presented elsewhere (*13*). Large, clearly resolved shifts on binding DNA are labeled. Several of these involve amino acid residues in the N-terminal extension to the core DNA-binding domain.

central four base pairs and in the flanking nucleotides (*3*, *7*, *32*). In a comparative binding study of the minimal DNA-binding domains, BPV-1 E2 appeared to be more forgiving as to the identity of the central nucleotides than HPV-16 E2 (*7*). When multiple isoforms of one protein or different proteins with a similar function participate in similar reactions, what factors govern the outcome? Could the binding preferences result from subtle conformational or surface amino acid residue differences between the different E2 proteins from different papillomaviral strains?

Solution NMR or X-ray crystallographic structures of the minimal DNA-binding domains from papillomaviral E2 protein are now known for three strains—HPV-16, HPV-31, and BPV-1. Comparison of the DNA-bound and DNA-free structures for BPV-1 yields two major conclusions (*3*−*5*). One, DNA binding is accompanied by small but significant tertiary structural changes in the protein and DNA. Two, reaction specificity may stem from charge distribution differences in proteins from different PV types and from flexibility inherent in the central nucleotide residues of the DNA. Structural flexibility in centrally located nucleotides would allow the DNA to bend around the protein. HPV-16 E2 is observed to have a much less electropositive surface than BPV-1 E2. Although the structure of the HPV-16 E2 complex with DNA is unknown, HPV-16 E2 would appear to be less able to use charge neutralization of phosphates to induce bending.

Stability Determining Structural Features in BPV-1 E2 DBD. Various constructs derived from internal restriction sites to the C-terminal end of the E2 gene have defined a C-terminal 85 residue core domain as the minimum required for DNA binding and dimerization (*33*). Treatment of full-length E2 with Pronase results in a proteolytically resistant core of ∼10 kDa (∼90 amino acid residues), but the exact boundaries of the domain were not defined (*34*). For the minimal BPV-1 E2 DBD, the equilibrium dissociation constants vary about 5-fold over a set of single DNA-binding sites, whereas for full-length E2 the equilibrium dissociation constants vary 300-fold (*7*, *35*). This suggests that the N-terminal extension to the minimal DNA-binding domain of BPV-1 E2 has a role in the protein's function. Mutational studies also suggest amino acid residues N-terminal to the core domain influence the ability of E2 to bind DNA (*11*). Two longer DBD constructs of BPV-1 E2, with either 101 or 125 residues, possess DNA-binding and protein stability characteristics that are better than that of the minimal domain (*11*). The structure of the 101 residue form of the DBD described here shows that the extra N-terminal residues interact with residues in the core domain, that the interactions are primarily hydrophobic in nature, and that a central cavity is protected from bulk solvent due to the interactions. These factors account for the observed increase in stability relative to the minimal domain.

The intersubunit or intermonomer interfaces of many proteins are hydrophobic, and many contain cavities (*36*). Similarly, the DNA-bound and DNA-free BPV-1 minimal E2 DBD structures contain a central cavity at the hydrophobic dimer interface (*2*, *3*). Small cavities are also observed in HPV-16 and in HPV-31 minimal DNA-binding domains (*4*, *5*). Water molecules are frequently found in intersubunit or interdomain cavities (*37*). A water molecule sits at the edge of either surface of the central cavity in BPV-1 E2 DBD

Table 3: Solvent-Accessible Surface Area of BPV-1 E2 DBD

surface area (Å^2)	dimer of 101 residues (obsd)[a]	core + extensions (calcd)[b]	difference[c]
total	3186	4070	884
hydrophobic	2144	2684	540
hydrophilic	1040	1384	344

[a] Solvent accessible surface area was calculated with a probe radius of 1.4 Å and is given for the dimeric form of the protein. [b] The surface area was calculated separately for residues 310−325 and for residues 326−410. The sum of these values represents the surface area expected when the two segments do not interact. [c] Additionally buried due to contacts between 16 residue extensions and the core 85 residue domain.

(*2*). The cavity in HPV-16 E2 DBD, although smaller, is proposed to accommodate a water molecule on the dimer 2-fold axis (*4*). In the structure, we have determined for the C-terminal 101 residues of BPV-1 E2 DBD that residues 318, 319, and 321 in the N-terminal extension pack against the cavity at the dimer interface. Urea-induced unfolding of BPV-1 E2 and HPV-16 E2 dimers to the unfolded monomers has been reported at a total protein concentration of 10 μM (*11*, *14*, *38*). The ΔG of unfolding for the 85 residue BPV-1 E2 DBD is 8.36 ± 0.29 kcal/mol and 12.97 ± 0.56 kcal/mol for the 101 residue form. For an 81 residue form of HPV-16 E2 DBD, it is 10.4 ± 0.52 kcal/mol (*14*, *38*). Therefore, the N-terminal extension on the minimal DBD of BPV-1 stabilizes the domain by 4.6 kcal/mol. The 101 residue form is more stable than the HPV-16 DBD by about 2.6 kcal/mol. The HPV-16 E2 DBD (and presumably HPV-31 E2) is more stable compared to the 85 residue form of BPV-1 E2 DBD, most likely due to its smaller internal cavity. The loss of the central cavity in the 101 residue form of BPV-1 E2 DBD, through protection by the N-terminal extension, leads to an increase in stability. These data suggest that stability of E2 increases when the cavity is filled. Scrutiny of the 101 residue form structure reveals that hydrophobic interactions between the N-terminal segment and the hydrophobic and aromatic side chains of core residues lining the central cavity are responsible for the greater stability.

We determined the extent of burial of hydrophobic surface area for BPV-1 E2 to assess the contribution to overall stability. Solvent-accessible surface areas were computed for the 85 residue dimeric core domain, the two 16 amino acid residue extensions, and for the 101 residue dimeric form (*39*) (Table 3). Comparison of the solvent-accessible surface areas reveals that 884 Å^2 of surface area are buried as the result of contacts between the two 16 N-terminal residue extensions and the 85 residue core domain of the dimer. A total of 540 Å^2 are hydrophobic and 344 Å^2 are hydrophilic. The free energy of burying 1 Å^2 of hydrophobic surface is estimated at 15−25 cal/mol, resulting in an expectation of about 8 kcal/mol of stabilization (*40*−*42*). This suggests that about 3.5 kcal/mol in destabilization may arise from loss of chain entropy and the burial of 344 Å^2 of hydrophilic surface yielding a net stabilization of ∼4.5 kcal/mol determined from unfolding data. In BPV-1 E2 DBD, hydrophobic interactions that lead to the loss of a central cavity stabilize the protein's structure, complementing the earlier findings on cavity-creating mutations that destabilize a protein (*43*, *44*).

Amide protons of about 25 core DBD residues, most of which are located in the β-barrel of BPV-1 E2, undergo slow hydrogen exchange ($k \leq 0.05$ h^{-1}), whereas those of the N-terminal residues exchange with solvent relatively fast ($k \geq 0.2$ h^{-1}) (data not shown). Thus, although residues 310−325 interact with the core domain in an intricate manner, they do not form a regular secondary structural element and exhibit some degree of increased mobility relative to the core residues of the DBD. This might also account for the observation that $\Delta\Delta G$ is approximately one-half of the expected change in free energy of stabilization. It is possible that some of the 16 N-terminal residues of each monomer form an additional β-strand either in the full-length E2 protein or when bound to DNA. If so, the hydrogen bonds are likely to form with the fourth β-strand (residues 400−410) of the other monomer and stabilize the protein by about 0.5 kcal/mol per hydrogen bond (*42*).

Comparison of Structure and Dynamics. The 101 residue form of BPV-1 E2 DBD reported here is similar in overall architecture to the other E2 DBD structures (Figure 5). Overall, structured regions of the core domain resemble the BPV-1 crystal structure (backbone RMS deviation of 1.5 Å on superimposing monomers) more closely than the HPV-31 solution structure (RMS deviation of 2.0 Å). Most of this difference results from the conformation of the two β-strands comprising the dimer interface centering on residues 400−410 (*4*, *5*). The NMR solution structure of the 101 residue form of BPV-1 E2 resembles the conformation found in the crystal structures of BPV-1 E2, rather than the somewhat different one found in either the NMR solution structure for HPV-31 E2 or the crystallographic structure of HPV-16 E2 (*3*−*5*). This suggests that the differences in conformation between BPV-1 and HPV-16 or HPV-31 E2 are due to differences in amino acid sequence rather than differences in structure determination technique.

Despite the fact that the HPV-31 and HPV-16 E2 proteins are about 32% identical in their sequences relative to the BPV-1, the proteins show some differences in binding DNA. The solution structure of the 85 residue minimal DBD of HPV-31 shows a similar overall architecture to the crystallographic structures for BPV-1 E2 DBD (Cα-trace RMS deviation of 1.3 Å). Yet, a systematic deviation was reported upon alignment of the backbone of monomers from these two structures (*5*). A small deviation was observed between the DNA-free and DNA-bound BPV-1 E2 minimal DBD (Cα-trace RMS deviation of 0.55 Å) and was suggested to reflect only the quaternary structural changes in the DBD resulting from DNA binding. The DNA recognition helices of the DNA-free protein are displaced away from the major groove relative to the helix in the protein−DNA complex (*3*). In the solution structure of the 101 residue form, the positions of the DNA-recognition helices appear somewhat shifted relative to the DNA-bound crystal structure, but toward the DNA rather than away (*3*−*5*). As previously observed in HPV-31 E2, the DNA helices (residues 333−349) are more flexible. In BPV-1 E2, all but two amide protons from the recognition helix exchange with deuterium within 20 h and several resonances gave very weak signals in the ^{15}N-separated NOESY spectrum. Amide resonances of several residues in the DNA-binding helix overlap with other amide resonances (*13*). The rapid amide exchange and resonance overlap led to fewer NOE-derived distances resulting in a less rigidly defined DNA-binding α-helix. Although the NOE-derived and coupling constant-derived

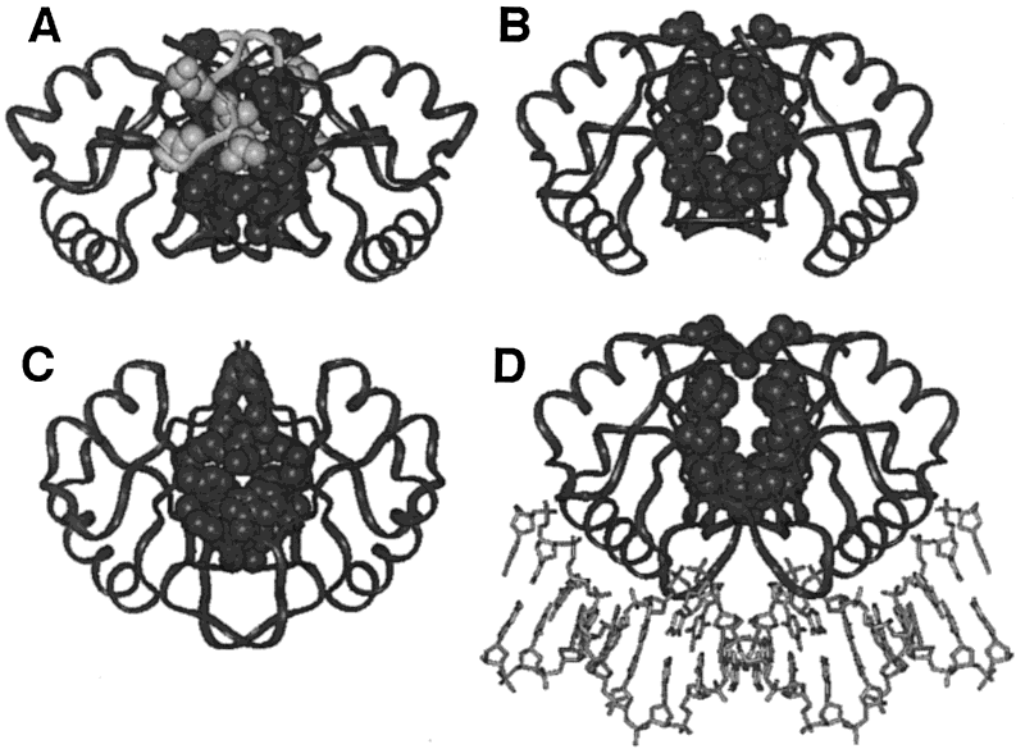

FIGURE 5: Comparison of papillomaviral E2 protein structures. The backbones of the models are shown as ribbons and residues in the dimer interface are shown in a space-filling format. The core domain residues are shown in dark gray, whereas the N-terminal extension is shown in light gray. (A) DNA-free NMR structure of BPV-1 E2 DBD (310−410); (B) DNA-free crystal structure of BPV-1 E2 DBD (326−410) (*2*); (C) DNA-free NMR structure of HPV-31 E2 DBD (*5*); (D) DNA-bound crystal structure of BPV-1 E2 DBD (326−410) (*2*). The DNA double helix is shown in stick format. Note the presence of a central cavity in the minimal BPV-1 E2 domains and masking of the cavity by residues in the N-terminal extension (panel A). The size of the cavity in HPV-16 E2 is similar to that in HPV-31 E2 (*4*).

data position the helices somewhat precisely (although less so than the rest of the molecule), on a relative slow time scale, there is likely a local breathing of the recognition helix (*5*). We agree with the conclusions of Liang et al. that this flexibility may facilitate an adjustment of the binding surface of the protein to achieve optimal interaction with DNA (*5*).

The dimeric E2 DBD is held together by hydrogen-bonding interactions between the backbone atoms of residues in the β-strands of the structural core and intricate intersubunit interactions between side chains of hydrophobic residues at the dimer interface. In BPV-1 E2, the protein core is sufficiently tightly packed with hydrophobic residues so that the Phe380 ring rotates slowly on the NMR time scale—separate resonances were observed for each of the ring protons (*13*). As with other E2 DBD structures determined in the absence of binding site DNA, residues 364−372 are part of an unstructured loop, as reflected by the low *S* values (see Supporting Information) and rapid amide exchange. Only in the presence of bound DNA does this loop become ordered due to contacts with nucleotide backbone (Figure 5).

Functional Significance of the Structure. In the X-ray structure for the core DBD−DNA complex (*2*), residues from the recognition helix (335−350) and the loop comprising residues 364−370 make direct contact with DNA. The NMR chemical shifts correspondingly change for these residues upon binding DNA (Figure 4). The loop, for example, is unstructured in the absence of DNA. When bound to DNA, the amide hydrogen of Ala364 makes a hydrogen bond with the carbonyl of residue Asp369, thus accounting for the nearly +1 ppm change in proton chemical shift.

The chemical shifts for several resonances in the dimer interface and N-terminal residues that interact with residues near the interface also are altered upon binding DNA. In particular, residues His319, Leu320, and Leu321, which form the flap over the central cavity, show chemical shift changes that indicates a perturbation in chemical environment when E2 binds DNA. Residues of the minimal core domain, Ala329, Leu330, Ile331, and Gly333 are positioned close to the residues in the N-terminal segment. They also undergo significant chemical shift changes, indicating that there is a change near the cavity on DNA binding which may involve a change in protein conformation or the interaction of protein with solvent. Residues 312−315, which are unstructured in the absence of DNA, also show chemical shift perturbations in agreement with our model that the N-terminal residues are positioned close to DNA. Although the new position of Asp316 in the presence of DNA could not be established unambiguously, its ^{1}H and ^{15}N resonances shift by at least 0.1 ppm (see Supporting Information), and residues flanking it show chemical shift changes when bound to DNA. This suggests an altered environment for Asp316.

Although parts of the 16 amino acid extension are unstructured, at least in the absence of DNA, we can speculate on the cause of the DNA-binding behavior of two E2 mutants. In BPV-1 E2 bearing an arginine replacement for cysteine 340, DNA binding is dependent on the presence of the N-terminal extension. Cysteine 340 makes two hydrogen bonds in the protein−DNA complex to the DNA (*2*). In the shortest 85 residue form, the mutant binds DNA with the same affinity as wild-type, probably by replacing the DNA base-specific contacts made by cysteine by favor-

able nonspecific contacts made by arginine. In the full-length and 125 residue forms, the Cys340 to Arg mutant is DNA-binding defective whereas the 101 residue form shows intermediate behavior (*11*). Residues 317−326 could place the N-terminal extensions near the DNA recognition helices (Figure 5A). Our model is that acidic residues contained in the N-terminal extension (residues 286−316) interact with arginine-340 in the mutant leading to the inability of the arginine to make nonspecific but stabilizing interactions with DNA (Figure 4). A second mutant that has aspartate 316 replaced by tyrosine abrogates DNA binding of E2, although the mutation is outside the core DNA-binding domain (*11*). Whereas wild-type E2 leads to a 280-fold increase in transactivation activity over a vector alone control, the Asp316 to Tyr mutant shows only a 2.8-fold increase (*11*). Although our model here is only speculative, it is possible for Asp 316 to hydrogen bond to Asn400 in the core domain. Replacement by the bulky tyrosine residue would presumably disrupt the structure of the core domain and interfere with DNA binding. Thus, specific residues adjacent to the minimal domain influence the DNA-binding function of the core domain.

To disrupt macromolecular interactions, stabilizing interactions must be overcome using chemical, physical, or other means. The present understanding of the stabilizing and destabilizing factors is seated in the combined empirical knowledge gained from mutational, thermodynamic, and structural analyses. The structures of the E2 DNA-binding domains provide a model for tailoring proteins for increased stability by reducing the size of a hydrophobic cavity. Delineation of these subtle structural differences and their contribution to stability and function are useful in protein design. The role of the N-terminal residues in HPV E2 DBD is not understood as well as they are with BPV-1 E2. Since the cavities at the dimer interfaces in HPV-16 and HPV-31 E2 are small, we predict that forms with N-terminal extensions will show little change in stability. The structure of the longer form of BPV-1 E2 DBD has provided information on structural features that impart additional stability relative to the minimal domain and has yielded insights that help in understanding the role of the N-terminal extension in DNA binding.

ACKNOWLEDGMENT

We acknowledge A. Bonvin and J. Caldwell for helpful hints on X-PLOR usage and D. Cullis for preparation of the partially ^{13}C-labeled protein. The ^{13}C-filtered, ^{13}C-edited HMQC-NOESY experiment was carried out at the Bruker facilities in Billerica with the help of C. Anklin.

SUPPORTING INFORMATION AVAILABLE

A figure showing the distributions of NOE cross-peaks per residue and angle order parameters for backbone ϕ and ψ angles and a table listing the ^{1}H and ^{15}N chemical shift changes in the backbone amides of E2 upon binding DNA (3 pages). This material is available free of charge via the Internet at http://pubs.acs.org.

REFERENCES

1. McBride, A. A., Byrne, J. C., and Howley, P. M. (1989) *Proc. Natl. Acad. Sci. U.S.A. 86*, 510−514.
2. Hegde, R. S., Grossman, S. R., Laimins, L. A., and Sigler, P. B. (1992) *Nature 359*, 505−512.
3. Hegde, R., Wang, A.-F., Kim, S.-S., and Schapira, M. (1998) *J. Mol. Biol. 276*, 797−808.
4. Hegde, R., and Androphy, E. J. (1998) *J. Mol. Biol. 284*, 1479−1489.
5. Liang, H., Petros, A. M., Meadows, R. P., Yoon, H. S. Y., Egan, D. A., Walter, K., Holzman, T. F., Robins, T., and Fesik, S. W. (1996) *Biochemistry 35*, 2095−2103.
6. Crothers, D. M. (1998) *Proc. Natl. Acad. Sci. U.S.A. 95*, 15163−5.
7. Hines, C. S., Meghoo, C., Shetty, S., Biburger, M., Brenowitz, M., and Hegde, R. S. (1998) *J. Mol. Biol. 276*, 809−818.
8. Bochkarev, A., Barwell, J. A., Pfuetzner, R. A., Bochkareva, E., Frappier, L., and Edwards, A. M. (1996) *Cell 84*, 791−800.
9. Bochkarev, A., Barwell, J. A., Pfuetzner, R. A., Furey, J., W., Edwards, A. M., and Frappier, L. (1995) *Cell 83*, 39−46.
10. Ambinder, R. F., Mullen, M. A., Chang, Y. N., Hayward, G. S., and Hayward, S. D. (1991) *J. Virol. 65*, 1466−78.
11. Pepinsky, R. B., Prakash, S. S., Corina, K., Grossel, M. J., Barsoum, J., and Androphy, E. J. (1997) *J. Virol. 71*, 828−831.
12. Lee, K. M., Androphy, E. J., and Baleja, J. D. (1995) *J. Biomol. NMR 5*, 93−96.
13. Veeraraghavan, S., Mello, C. C., Lee, K. M., Androphy, E. J., and Baleja, J. D. (1998) *J. Biomol. NMR*, 457−458.
14. Mok, Y.-K., Prat Gay, G. d., Butler, P. J., and Bycroft, M. (1996) *Protein Sci. 5*, 310−319.
15. Vuister, G. W., Kim, S.-J., Wu, C., and Bax, A. (1994) *J. Am. Chem. Soc. 116*, 9206−9210.
16. Wishart, D. S., Bigam, C. G., Yao, J., Abildgaard, F., Dyson, H. J., Oldfield, E., Markley, J. L., and Sykes, B. D. (1995) *J. Biomol. NMR 6*, 135−140.
17. Veeraraghavan, S., Gilbert, G. D., and Baleja, J. D. (1998) *Biochem. J. 332*, 549−555.
18. Wagner, G., Braun, W., Havel, T. F., Schaumann, T., Go, N., and Wüthrich, K. (1987) *J. Mol. Biol. 196*, 611−639.
19. Wüthrich, K. (1986) *NMR of Proteins and Nucleic Acids*, pp 130−161, Wiley-Interscience, New York.
20. Szyperski, T., Güntert, P., Otting, G., and Wüthrich, K. (1992) *J. Magn. Reson. 99*, 552−560.
21. Neri, D., Szyperski, T., Otting, G., Senn, H., and Wüthrich, K. (1989) *Biochemistry 28*, 7510−7516.
22. Hyberts, S. G., Märki, W., and Wagner, G. (1987) *Eur. J. Biochem. 164*, 625−635.
23. Wishart, D. S., and Sykes, B. D. (1994) *J. Biomol. NMR 4*, 171−180.
24. Wishart, D. S., Sykes, B. D., and Richards, F. M. (1992) *Biochemistry 31*, 1647−1651.
25. MacKerell, A. D., Bashford, D., Bellott, M., Dunbrack, R. L., Evanseck, J. D., Field, M. J., Fischer, S., Gao, J., Guo, H., Ha, S., Joseph-McCarthy, D., Kuchnir, L., Kuczera, K., Lau, F. T. K., Mattos, C., Michnick, S., Ngo, T., Nguyen, D. T., Prodhom, B., Reiher, W. E., Roux, B., Schlenkrich, M., Smith, J. C., Stote, R., Straub, J., Watanabe, M., Wiorkiewicz-Kuczera, J., Yin, D., and Karplus, M. (1998) *J. Phys. Chem. B 102*, 3586−3616.
26. Brooks, B. R., Bruccoleri, R. E., Olafson, B. D., States, D. J., Swaminathan, S., and Karplus, M. (1983) *J. Comput. Chem. 4*, 187−217.
27. Hyberts, S. G., Goldberg, M. S., Havel, T. F., and Wagner, G. (1992) *Protein Sci. 1*, 736−751.
28. Laskowski, R. A., Macarthur, M. W., Moss, D. S., and Thornton, J. M. (1993) *J. Appl. Crystallogr. 26*, 283−291.
29. Edsall, J. T., and Wyman, J. (1958) *Biophysical Chemistry*, pp 406−476, Academic Press, New York.
30. Matthews, B. W. (1995) in *Advances in Protein Chemistry* (Anfinsen, C. B., Edsall, J. T., Richards, F. M., and Eisenberg, D. S., Eds.) pp 249−278, Academic Press, San Diego, CA.
31. Shortle, D. (1995) in *Advances in Protein Chemistry* (Anfinsen, C. B., Edsall, J. T., Richards, F. M., and Eisenberg, D. S., Eds.) pp 214−247, Academic Press, San Diego, CA.

32. Thain, A., Webster, K., Emery, D., Clarke, A. R., and Gaston, K. (1997) *J. Biol. Chem. 272*, 8236−8242.
33. Monini, P., Grossman, S. R., Pepinsky, B., Androphy, E. J., and Laimins, L. A. (1991) *J. Virol. 65*, 2124−2130.
34. Dostatni, N., Thierry, F., and Yaniv, M. (1988) *EMBO J. 7*, 3807−3816.
35. Li, R., Knight, J., Bream, G., Stenlund, A., and Botchan, M. (1989) *Genes Dev. 3*, 510−526.
36. Larsen, T. A., Olson, A. J., and Goodsell, D. S. (1998) *Structure 6*, 421−7.
37. Hubbard, S. J., and Argos, P. (1994) *Protein Sci. 3*, 2194−2206.
38. Mok, Y.-K., Bycroft, M., and de Prat-Gay, G. (1996) *Nat. Struct. Biol. 3*, 711−717.
39. Islam, S. A. (1993) PDBAREA, Imperial Cancer Research Fund, England.
40. Eisenhaber, F. (1996) *Protein Sci. 5*, 1676−86.
41. Vallone, B., Miele, A. E., Vecchini, P., Chiancone, E., and Brunori, M. (1998) *Proc. Natl. Acad. Sci. U.S.A. 95*, 6103−7.
42. Honig, B., and Yang, A. S. (1995) in *Advances in Protein Chemistry* (Anfinsen, C. B., Edsall, J. T., Richards, F. M., and Eisenberg, D. S., Eds.) pp 27−58, Academic Press, San Diego, CA.
43. Eriksson, A. E., Baase, W. A., Zhang, X. J., Heinz, D. W., Blaber, M., Baldwin, E. P., and Matthews, B. W. (1992) *Science 255*, 178−83.
44. Vlassi, M., Cesareni, G., and Kokkinidis, M. (1999) *J. Mol. Biol. 285*, 817−27.

BI991633X